The International Journal of Advanced Manufacturing Technology (2023) 125:1493–1509
https://doi.org/10.1007/s00170-022-10788-x

ORIGINAL ARTICLE

Parameters affecting the quality of friction drilled holes and formed thread in austenitic stainless steel AISI 304

Nada Abdelmoneim Bassiouny[1] · Mohammad Al-Makky[1] · Helmi Youssef[1]

Received: 6 September 2022 / Accepted: 27 December 2022 / Published online: 9 January 2023

Abstract
The main purpose of this research paper is to improve the quality of the friction-drilled holes and formed thread by investigating the influence of the input working parameters that have not been investigated yet on the quality of the produced bores. Due to lack of research related to the hardness macro- and microstructure of formed threads, experiments were conducted to investigate these important issues. Finally, a tension test was performed to compare the performance of the form tapped thread with the conventionally cut thread. The experiments were conducted on difficult-to-cut material AISI 304 stainless steel workpieces with (2 and 3 mm) wall thicknesses. Tungsten carbide friction drills with diameters (Ø9.2, Ø7.3, and Ø4.5 mm) were used to perform the experiments. The effects of the ratio of workpiece thickness (t) to tool diameter (d_T), rotational speed (N), and feed speed (f) on the hole diametral oversize (U), cylindricity error, and collar height were studied. The analysis of variance (ANOVA) showed that the t/d ratio was the most significant factor affecting the mean cylindricity error and the collar height. By comparing the performance of the three tools, it was noticeable that the friction drill Ø7.3 realized better results in terms of mean hole diametral oversize and mean cylindricity error. The elevated temperature associated with high plastic deformation during the processes resulting in fine grains with high hardness values were observed at the heat-affected zone. The longer effective thread length of the formed thread realized higher strength values than the cut thread.

Keywords Friction drilling · Form tapping · Hole diametral oversize · Cylindricity error · Microstructure · Tension test

1 Introduction

Friction drilling is a novel, promising hole-making process compared to cutting or conventional hole-making processes. Materials like stainless steels are characterized by high toughness, low thermal conductivity, and high work-hardening coefficient. These characteristics make stainless steels hard to machine, and friction drilling offers in this case the solution.

Friction drilling is distinguished by being dry and clean without applying coolant or generating chips (chip-less process). The friction drilling process depends on the heat generated from the friction force between the rotating conical tool and the workpiece. This leads to a temperature rise of about half and two-thirds of the melting temperature of the work material, causing a decrease in the yielding point and softening of the work material, hence facilitating the plastic deformation to form the bushing [1]. As the friction drill penetrates and pushes the material, some of the extruded material forms a collar around the upper surface of the workpiece, and the rest forms a bushing in the lower surface of the workpiece, as illustrated in Fig. 1. All this happens in a matter of seconds. All work material from the hole contributes to forming the collar and the bushing. The produced bushing and collar (L_b) are 2 to 4 times the workpiece wall thickness (t), thus increasing the effective thread length and joint strength of the tapped joint [2]. Friction drilling solves the problem of screw connections at thin-wall thicknesses and replaces the welding nuts or attaching rivet nuts.

The hole quality is an essential characteristic that incorporates geometrical properties, the material structure at various hierarchical levels, and imperfections. Chow et al.,

✉ Nada Abdelmoneim Bassiouny
nada.abdelmoniem@alexu.edu.eg

Mohammad Al-Makky
m.almakky@alexu.edu.eg

Helmi Youssef
helmi.youssef@alexu.edu.eg

[1] Production Engineering Department, Faculty of Engineering, Alexandria University, Alexandria, Egypt

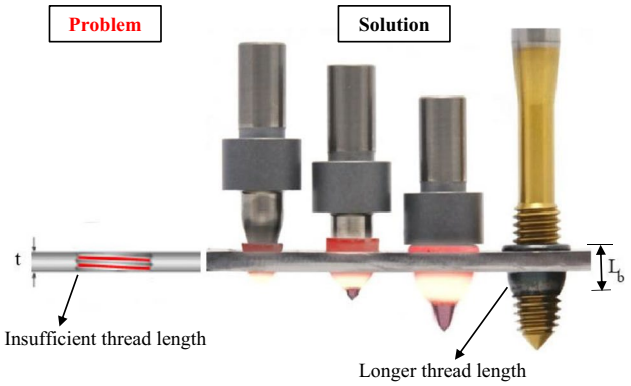

Fig. 1 Illustration of friction drilling and form tapping processes steps, showing the problem, and solution

Ku et al., and El-Bahloul et al. [3–6] studied the effect of process parameters such as rotational speed, feed rate, friction tool angle, and friction contact area ratio while friction drilling AISI 304 stainless steel sheets using a tungsten carbide tool. The results revealed that the values of roundness error were very small compared to diameter dimensional error; the friction angle and spindle speed were the most significant factors affecting the surface roughness, and the bushing length was only affected by the friction contact area ratio. Dehghan et al. [7] performed a comparative study of AISI304, Ti-6Al-4 V, and Inconel718 to study the effect of process parameters (spindle speed and feed rate) experimentally and numerically on bushing shape and height, hardness, thermal stress, heat generation, hole roundness, and tool performance. Inconel718 achieved a higher bushing formation quality and tool performance than AISI304 and Ti-6Al-4 V. However, AISI304 and Inconel718 had the highest hardness because of low thermal conductivity. Sobotová et al., Somasundaram et al., Ozler et al., Demir et al., and Ozek et al. [1, 8–11] explored the influence of process parameters on the hole quality of the produced bushings.

Many authors investigated the friction drilling process, but there are limited studies about the form tapping process. Like, Urbikain et al. [12] joined sheets and tubes made from couples of dissimilar materials using a combined friction drilling and form tapping method. Mechanical and corrosion tests showed that the new joints had similar properties and collapsed under similar stress thresholds to traditional cutting processes. Sarafraz et al. [13] used different twist drill diameters to investigate the influence of pre-drilling AZ91 magnesium cast alloys on the hardness and tensile failure of the obtained formed threads. The results revealed that the increase in pre-drilling diameter led to a reduction in hardness in the thickness direction, and the oversize of the friction drilled bores increased. However, variations of the pre-drilling diameter did not reveal a definite trend in obtained tensile strengths caused by inadequate thread profile formation. Wu et al. [14] compared four threaded holes of 6082-T6 aluminum alloy combinations of friction drilling and twit drilling followed by thread forming and thread cutting. A test procedure was developed to measure the axial load-bearing capacity in threaded joints. The results clarified that the threaded holes made by friction drilling and thread forming achieved a 35% increase in peak load compared to threaded holes made by conventional twist drilling. Thread stripping Factors of Safety were obtained to safeguard against internal thread stripping in thin-walled structures must be in the range of 3.61 to 4.38 to give reliability of 95% to 99.9% against thread stripping in friction drilled and thread-formed joints.

Miller et al. [15] mentioned that the ratio of workpiece thickness (t) to tool diameter (d_T) is a vital parameter in friction drilling. A high t/d ratio indicates that a large amount of material is extruded and formed in the bushing. The t/d is 0.75 for cast metals, higher than 0.16 for the AISI 1020 steel. Based on the literature, there is no available study to investigate the process parameter t/d ratio on the hole quality, especially for materials difficult to cut, like AISI 304 stainless steel. Moreover, it is difficult to find a comparison between the form tapped joint and the conventional tapped joint regarding the ultimate tensile load.

Consequently, the main purpose of this study was to investigate the effect of t/d ratio, rotational speed (N), and feed speed (f) on the hole quality, such as hole diametral oversize (U), cylindricity error, and collar height. Moreover, the most significant factor was specified by Minitab 19 software in friction drilling for AISI 304 stainless steel specimens with different wall thicknesses using three different diameters of carbide tools. A vital factor in friction drilling is the following process of thread forming. Therefore, the quality of the formed thread was investigated in terms of hardness and revealed microstructure. A comparison in the performance between form tapping and conventional cut tapping was also performed. Figure 2 illustrates the friction drilling process and the produced bushing, where t is the workpiece thickness, h is the collar height, d_T and d_H are the tool, and the measured hole diameters.

2 Experimental procedure

2.1 Friction drilling and form tapping machines

An LMV850 three-axis CNC vertical machining center was used for friction drilling of the AISI 304 stainless steel specimens, as shown in Fig. 3. The tool was clamped to a tool holder consisting of a transmission shaft, collet,

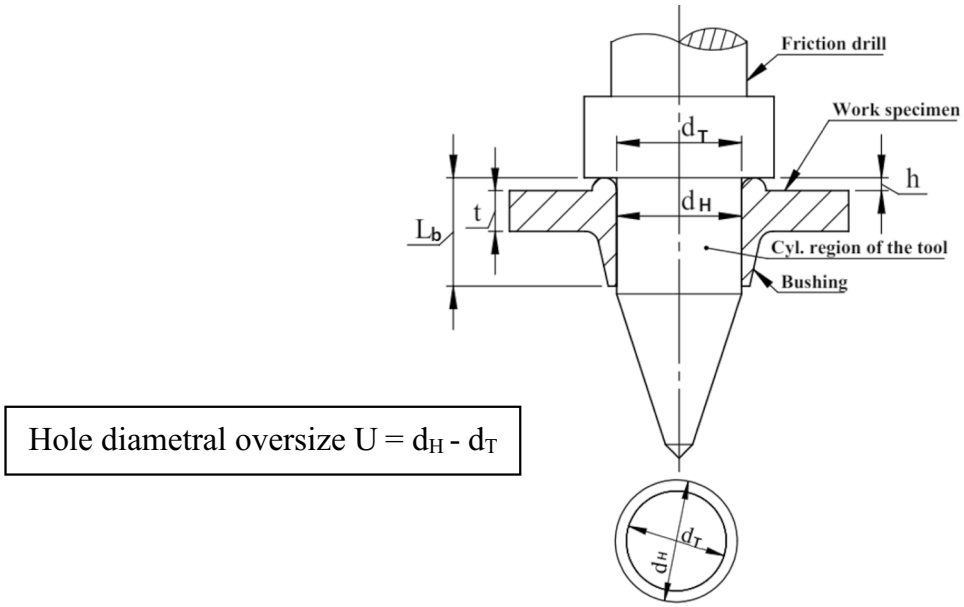

Fig. 2 Schematic drawing showing metal deformation and hole diametral oversize in the friction drilling process

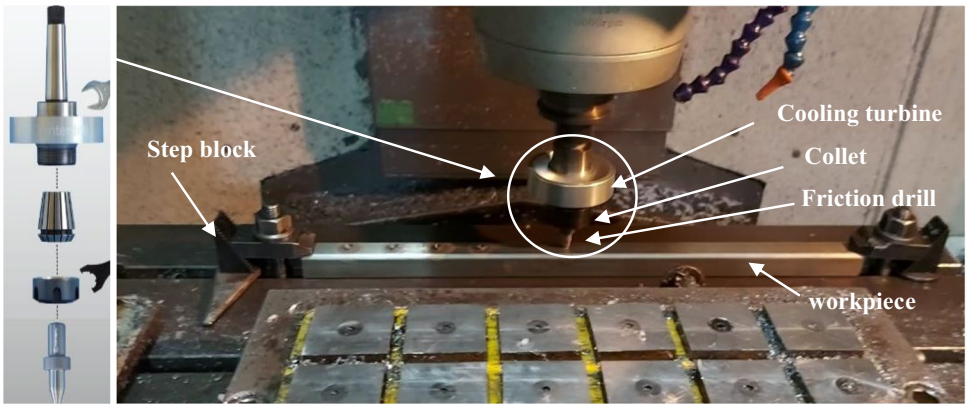

Fig. 3 Friction drilling experimental setup

clamping nut, and a cooling turbine to dissipate the generated heat effectively, thus preventing the machine spindle from being damaged.

After the friction drilling process, form tapping was conducted using different form taps on a conventional upright drilling machine, shown in Fig. 4. An oil lubricant was used during this process before tapping each hole to prevent galling and guarantee a high quality of the formed threads.

2.2 Work specimens

In this study, two specimens with a square cross-sectional area of 25 mm × 25 mm and 500 mm length were used. However, the specimens have different wall thicknesses, specimen A has 2 mm, and specimen B has a 3-mm wall thickness, as illustrated in Fig. 5. The chemical analysis was performed by a spectrometer, and the results are recorded in Table 1. Both specimens are austenitic stainless steel AISI 304.

2.3 Friction drilling tools

Three friction drilling tools were used to conduct these experiments. They are made of tungsten carbide grains in a cobalt matrix. The tools are of Ø4.5-mm, Ø7.3-mm, and Ø9.2-mm diameters, as shown in Fig. 6. Tool Ø7.3 (M8) was offered by Formdrill company in Belgium; however, the others were locally manufactured by Noval Tools, an Egyptian manufacturer of cutting tools. The diameters of the friction drills were selected to produce internal threads M5 × 0.8, M8 × 1.25, and M10 × 1.5, respectively, by form tapping processes.

2.4 Form taps

Taps with different cross-sections and dimensions were used to tap threads, as illustrated in Table 2. All taps are made of high-speed steel tap M8 × 1.25 and M5 × 0.8 coated by titanium nitride (TiN) coating; however, tap M10 × 1.5 is uncoated. The TiN coating provides high

Fig. 4 Form tapping experimental setup

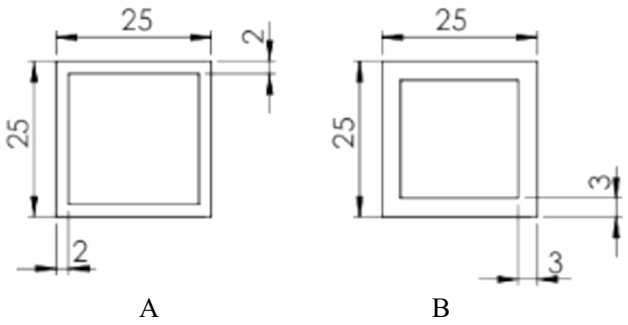

Fig. 5 **A**, **B** Geometrical dimensions of work specimens

wear resistance to increases the tool life. All taps have an approach thread length. Tap M5 × 0.8 is provided by the Germany Centerdrill company; however, tap M10 × 1.5 is made in Germany, and tap M8 × 1.25 is offered by the Belgium Formdrill company. All taps are manufactured according to DIN 13–1 and ISO 68 standards.

3 Fractional factorial design

A fractional factorial design was applied to design the experiments to reduce the number of experiments, and the process parameters were comprehensively investigated. Twenty-four experiments were conducted, 12 experiments for each of specimens A and B. The experiments were conducted as follows ($2^{k-1} = 2^{3-1} = 4$ *runs*) with two replications for each used tool to decrease the experimental error. These experiments were designed to study the effect of the *t*/*d* ratio, the rotational speed, and the feed rate on the investigated responses. These responses were the hole diametral oversize, collar height, and cylindricity error of the produced bushings.

Table 3 indicates the input working parameters and their levels for each tool. The levels were selected as recommended by the tool manufacturers. The produced hole diameter and cylindricity error were measured by the coordinate measuring machine (Contura select by Carl Zeiss). However, the collar height was measured from the top-hole edge to the specimen top surface by a Toolmaker microscope. Table 4 indicates the performed experimental plans for holes Ø 4.5, Ø 7.3, and Ø 9.2, respectively.

The form tapping process was then conducted according to the input working parameters given in Table 5. A hardness test was performed to investigate the micro-hardness of the formed thread cross-section. The specimen was evaluated using the LM-100 micro-hardness tester. The thread microstructure was observed by scanning electron microscope (JSM-IT200) and the macrostructure by stereo optical microscope (MEIJI EMZ-5). Finally, a mechanical tensile test was performed by a universal testing machine to compare the formed thread with the conventional cutting thread.

Table 1 Chemical composition of AISI 304 stainless steel work specimens

Specimen	C %	Si %	Mn %	P %	S %	Mo %	Cr %	Ni %	Fe %
A	0.086	0.38	0.92	0.011	0.001	0.059	18.584	9.692	71.966
B	0.043	0.44	1.43	0.011	0.001	0.126	18.363	9.152	71.523

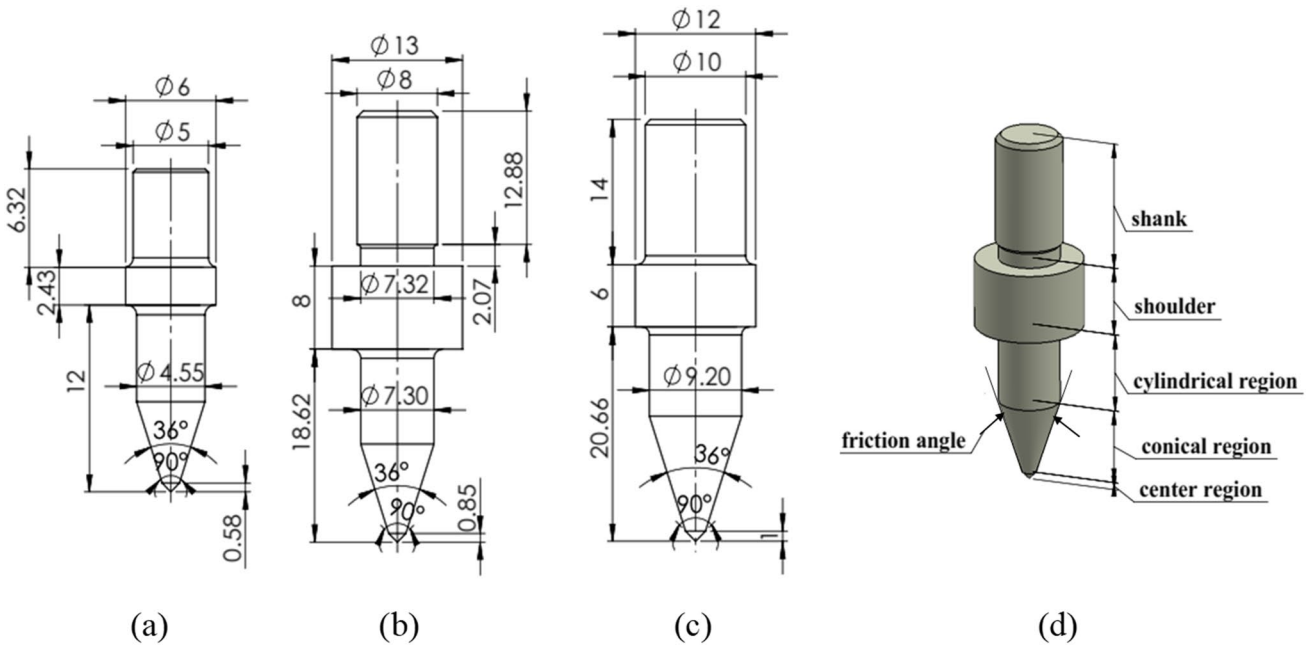

Fig. 6 Geometrical dimensions of friction drilling tools. a Ø4.5 (M5), b Formdrill tool Ø7.3 (M8), c Ø9.2 (M10), d tool geometry

Table 2 The geometry of used form taps

M10x1.5			**Six lobes**
M8x1.25			**Five lobes**
M5x0.8			**Four lobes**

Table 3 Working parameters and their levels by the friction drilling process

	Tool Ø 4.5 (M5)		Tool Ø7.3 (M8)		Tool Ø9.2 (M10)	
Levels	Low	High	Low	High	Low	High
t/*d* ratio	0.44	0.67	0.27	0.41	0.22	0.33
Rotational speed *N* (rpm)	2200	2800	1800	2400	1600	2200
Feed speed *f* (mm/min)	50	150	50	150	50	150

*The levels of N and f are recommended by the tool manufacturers.

Table 4 Experimental plan for the friction drilling process

Standard order	Friction drill diameter (mm)	Specimen	*t*/*d* ratio	Rotational speed *N* (rpm)	Feed speed *f* (mm/min)
1	Ø4.5	A	0.44	2200	150
2	Ø4.5	B	0.67	2200	50
3	Ø4.5	A	0.44	2800	50
4	Ø4.5	B	0.67	2800	150
5	Ø4.5	A	0.44	2200	150
6	Ø4.5	B	0.67	2200	50
7	Ø4.5	A	0.44	2800	50
8	Ø4.5	B	0.67	2800	150
9	Ø7.3	A	0.27	1800	150
10	Ø7.3	B	0.41	1800	50
11	Ø7.3	A	0.27	2400	50
12	Ø7.3	B	0.41	2400	150
13	Ø7.3	A	0.27	1800	150
14	Ø7.3	B	0.41	1800	50
15	Ø7.3	A	0.27	2400	50
16	Ø7.3	B	0.41	2400	150
17	Ø9.2	A	0.22	1600	150
18	Ø9.2	B	0.33	1600	50
19	Ø9.2	A	0.22	2200	50
20	Ø9.2	B	0.33	2200	150
21	Ø9.2	A	0.22	1600	150
22	Ø9.2	B	0.33	1600	50
23	Ø9.2	A	0.22	2200	50
24	Ø9.2	B	0.33	2200	150

Table 5 Working parameters for conventional drilling, cut, and form tapping processes

Twist drilling				Cut tapping	Form tapping
Twist drill diameter	Rotational speed *N* (rpm)	Feed rate f_r (mm/rev)	Tap	Rotational speed *N* (rpm)	Rotational speed *N* (rpm)
Ø 4.2	710	0.08	M5 × 0.8	450	280
Ø 6.8	450	0.12	M8 × 1.25	280	180
Ø 8.5	450	0.12	M10 × 1.5	180	180

*The selected *N* and f_r are recommended by the tool manufacturers.

4 Results and discussion

4.1 Mean hole diametral oversize difference

The mean hole diametral oversize was calculated by subtracting the measured tool diameter (d_T) from the measured hole diameter (d_H), Fig. 2.

The results were analyzed in Tables 6, 7, and 8 then plotted in Fig. 7. Pareto charts illustrate that the only significant factor is the rotational speed for holes Ø9.2 and the *t*/*d* ratio for holes Ø7.3; however, for holes Ø4.5, all factors are non-significant. The main effect plots reveal

Table 6 ANOVA for mean hole diametral oversize for holes Ø4.5

Source	DF	Adj SS	Adj MS	*F*-value	*P*-value
Model	3	0.000689	0.000230	0.22	0.879
Linear	3	0.000689	0.000230	0.22	0.879
t/*d*	1	0.000481	0.000481	0.46	0.535
N (rpm)	1	0.000000	0.000000	0.00	0.989
f (mm/min)	1	0.000208	0.000208	0.20	0.679
Error	4	0.004189	0.001047		
Total	7	0.004878			

Model summary: $S = 0.0323623$, R-sq = 14.12%, R-sq(adj) = 0.00%, R-sq(pred) = 0.00%

Table 7 ANOVA for mean hole diametral oversize for holes Ø7.3

Source	DF	Adj SS	Adj MS	*F*-value	*P*-value
Model	3	0.010427	0.003476	5.76	0.062
Linear	3	0.010427	0.003476	5.76	0.062
t/d	1	0.010182	0.010182	16.87	0.015
N (rpm)	1	0.000020	0.000020	0.03	0.863
f (mm/min)	1	0.000225	0.000225	0.37	0.575
Error	4	0.002414	0.000603		
Total	7	0.012841			

Model summary: $S = 0.0245652$, R-sq = 81.20%, R-sq(adj) = 67.10%, R-sq(pred) = 24.81%

Table 8 ANOVA for mean hole diametral oversize for holes Ø9.2

Source	DF	Adj SS	Adj MS	*F*-value	*P*-value
Model	3	0.002294	0.000765	9.49	0.027
Linear	3	0.002294	0.000765	9.49	0.027
t/d	1	0.000032	0.000032	0.39	0.565
N (rpm)	1	0.002261	0.002261	28.05	0.006
f (mm/min)	1	0.000002	0.000002	0.02	0.897
Error	4	0.000322	0.000081		
Total	7	0.002617			

Model summary: $S = 0.0089785$, R-sq = 87.68%, R-sq(adj) = 78.44%, R-sq(pred) = 50.71%

that the mean hole diametral oversize decreases by increasing the *t/d* ratio, rotational speed (*N*), and feed speed (*f*) for all tested holes. For holes Ø7.3, an increase of the *t/d* ratio from 0.27 to 0.41 leads to a decrease in the mean hole diametral oversize by 86.22%. Increasing the *t/d* ratio means that a large amount of the work material is formed, resulting in more frictional heat, which softens and easily deforms the work material; therefore, the mean hole oversize decreases. For holes Ø9.2, when the rotational speed increases from 1600 to 2200 rpm, the mean hole diametral oversize decreases by 32.68%. The increase of rotational speed generates more frictional heat, reducing the mean hole diametral oversize.

It is noticeable that the tool diameter Ø7.3 achieves the lowest mean hole oversize of 0.047 mm as compared to 0.086 mm and 0.077 mm for holes Ø9.2 and Ø4.5, respectively, as shown in Fig. 8. Those values represent the mean of 8 experiments for each hole diameter. Formdrill tool Ø7.3 imported from Belgium is performed better than the locally manufactured tools Ø4.5 and Ø9.2 because of the high quality of the friction drill Ø7.3.

The tool overhang ratio is the ratio of the tool diameter to the tool length extended from the end of the tool holder. It was found that Formdrill tool Ø7.3 has the least overhang ratio, equal to 0.27 compared to other tools, 0.35 and 0.32 for tools Ø9.2 and Ø4.5, respectively, which makes the tool

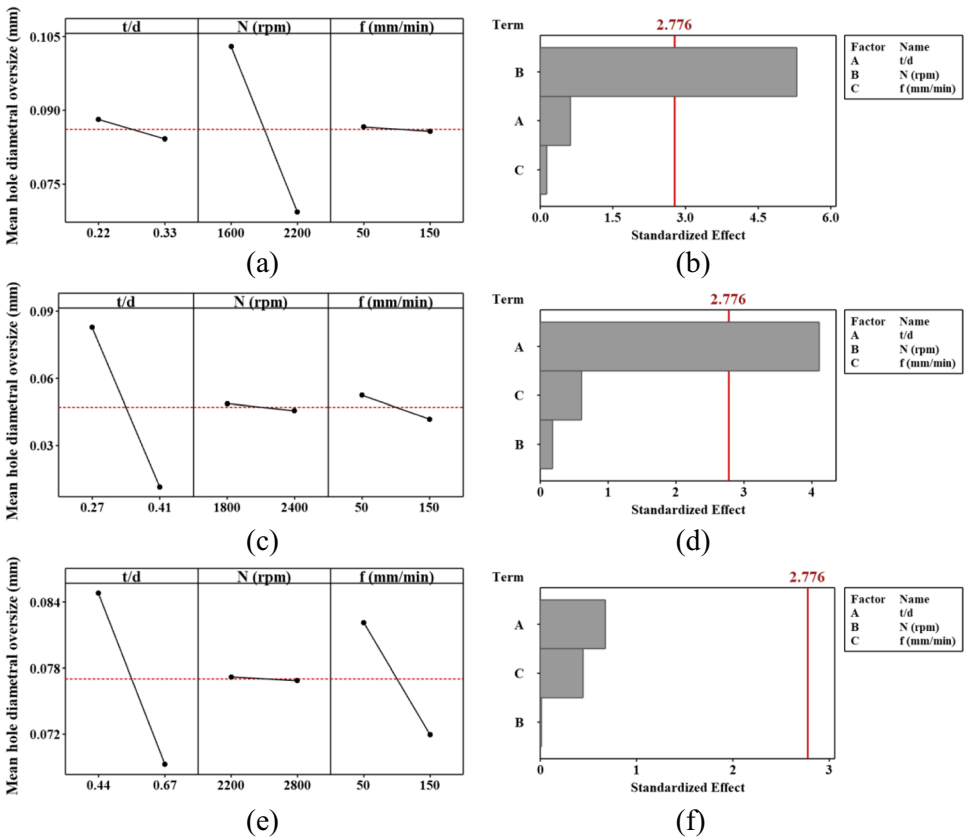

Fig. 7 Main effects plots and Pareto chart of the effets plots for mean hole diametral oversize. a Main effect plot for holes Ø9.2. b Pareto chart of standardized effect for holes Ø9.2. c Main effect plot for holes Ø7.3. d Pareto chart of standardized effect for holes Ø7.3. e Main effect plot for holes Ø4.5. f Pareto chart of standardized effect for holes Ø4.5

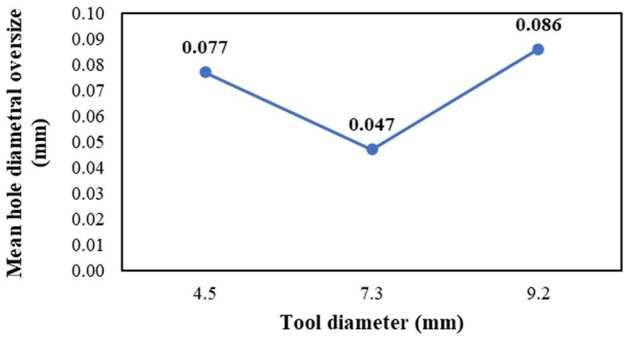

Fig. 8 Effect of different friction drills on the mean hole diametral oversize

more stable by reducing chatter and vibration. Therefore, it realized the lowest mean hole diametral oversize.

4.2 Mean cylindricity error

The CMM scanning probe passed over the hole surface in a spiral movement toward the hole outlet side. Data collected was evaluated by the minimum zone cylinder criteria based on the reference cylinders, as shown in Fig. 9. A reference cylinder was first obtained using the data measured from the hole surface. The measured points were then compared with the reference cylinder. Therefore, Calypso 4.0 software calculated the hole cylindricity error based on the minimum radial separation between the two concentric reference cylinders where all data must lie.

Then, an analysis of variance for hole cylindricity error was conducted, as given in Tables 9, 10, and 11, and the results are illustrated in Fig. 10. Pareto charts show that the *t/d* ratio is the only significant factor, while the rotational speed and the feed speed are non-significant factors on the cylindricity error. The main effect plots illustrate that the three factors (*t/d*, *N*, and *f*) are directly proportional to the cylindricity error.

Table 9 ANOVA for mean cylindricity error for holes Ø4.5

Source	DF	Adj SS	Adj MS	*F*-value	*P*-value
Model	3	0.044002	0.014667	26.96	0.004
Linear	3	0.044002	0.014667	26.96	0.004
t/d	1	0.037019	0.037019	68.05	0.001
N (rpm)	1	0.002843	0.002843	5.23	0.084
f (mm/min)	1	0.004141	0.004141	7.61	0.051
Error	4	0.002176	0.000544		
Total	7	0.046178			

Model summary: $S = 0.0233234$, R-sq = 95.29%, R-sq(adj) = 91.75%, R-sq(pred) = 81.15%

Table 10 ANOVA for mean cylindricity error for holes Ø7.3

Source	DF	Adj SS	Adj MS	*F*-value	*P*-value
Model	3	0.009485	0.003162	4.32	0.096
Linear	3	0.009485	0.003162	4.32	0.096
t/d	1	0.009316	0.009316	12.72	0.023
N (rpm)	1	0.000007	0.000007	0.01	0.926
f (mm/min)	1	0.000162	0.000162	0.22	0.663
Error	4	0.002930	0.000733		
Total	7	0.012415			

Model summary: $S = 0.0270650$, R-sq = 76.40%, R-sq(adj) = 58.70%, R-sq(pred) = 5.60%

For the holes Ø9.2, when the *t/d* ratio rises from 0.22 to 0.33, the mean value of the cylindricity error increases from 0.0705 to 0.161 mm. For the holes Ø7.3, an increase of the *t/d* ratio from 0.27 to 0.41 leads to an increase in the mean cylindricity error from 0.022 to 0.0902 mm. However, for the holes Ø4.5, the cylindricity error increases from 0.0354 to 0.1715 mm when the *t/d* ratio increases from 0.44 to 0.67. Figure 11 illustrates that the holes Ø7.3 achieve the minimum mean cylindricity error compared to

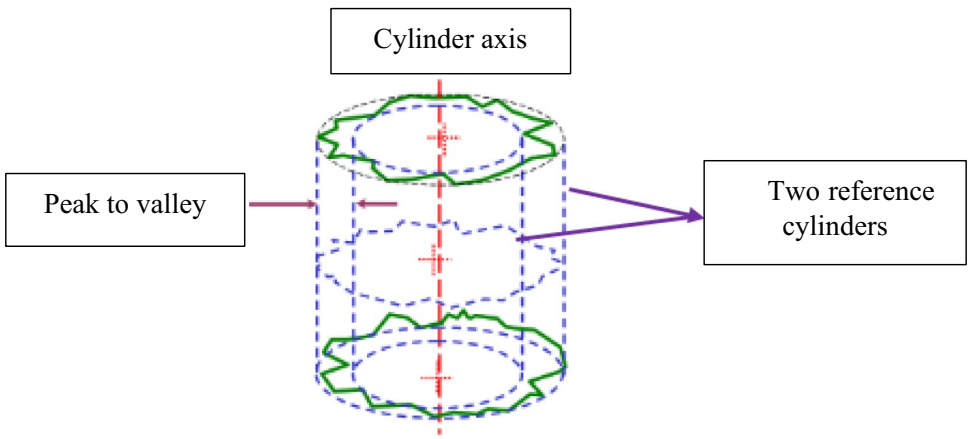

Fig. 9 Minimum zone cylinder (MZC) method to evaluate the cylindricity error

Table 11 ANOVA for mean cylindricity error for holes Ø9.2

Source	DF	Adj SS	Adj MS	*F*-value	*P*-value
Model	3	0.016526	0.005509	13.76	0.014
Linear	3	0.016526	0.005509	13.76	0.014
t/d	1	0.016308	0.016308	40.72	0.003
N (rpm)	1	0.000035	0.000035	0.09	0.781
f (mm/min)	1	0.000182	0.000182	0.46	0.537
Error	4	0.001602	0.000400		
Total	7	0.018128			

Model summary: $S = 0.0200113$, R-sq = 91.16%, R-sq(adj) = 84.54%, R-sq(pred) = 64.65%

those resulting from the holes Ø9.2 and Ø4.5. As a result of the tool overhang, which produces tool chattering and vibration, therefore, the mean cylindricity error increases.

The increasing trend of the mean hole cylindricity error indicates that the increasing feed decreases the contact time of the tool with the workpiece, causing more force for penetration. Therefore, the axial force increases associated with vibrations, increasing the cylindricity error. The cylindricity error increases at high spindle speed owing to tool skidding. Moreover, when the *t/d* ratio increases, the axial force increases, which enhances cylindricity error [16].

4.3 Collar height

Analysis of variance for collar height (h) was performed, as given in Tables 12, 13, and 14; the results are shown in Fig. 12. Pareto charts reveal that the three factors (*t/d*, *N*, and *f*) are significant; however, the *t/d* ratio is the most significant factor for all holes, then the feed and the rotational speed. The main effect plots clarify that the collar height increases by increasing the *t/d* ratio, rotational speed, and feed speed. As a result, for holes Ø9.2, by raising the *t/d* ratio from 0.22 to 0.33, the collar height increases by 67.32%. However, it increases by increasing rotational speed from 1600 to 2200 rpm, about 11.26%, and by increasing feed speed from 50 to 150 mm/min, about 21.02%. For holes Ø7.3, the collar height increases by 18.79% when the *t/d* ratio increases from 0.27 to 0.41. Nevertheless, it increases by 4.98% as the rotational speed increases from 1800 to 2400 rpm and by 6.35% when the feed speed increases from 50 to 150 mm/min. For holes Ø4.5, the collar height increases by increasing the three factors (*t/d* ratio, rotational speed, and feed speed) by 12.04%, 4.46%, and 2.65%, respectively. Figure 13 illustrates that increasing the tool diameter leads to an increase in the collar height because the amount of material that will be deformed becomes larger.

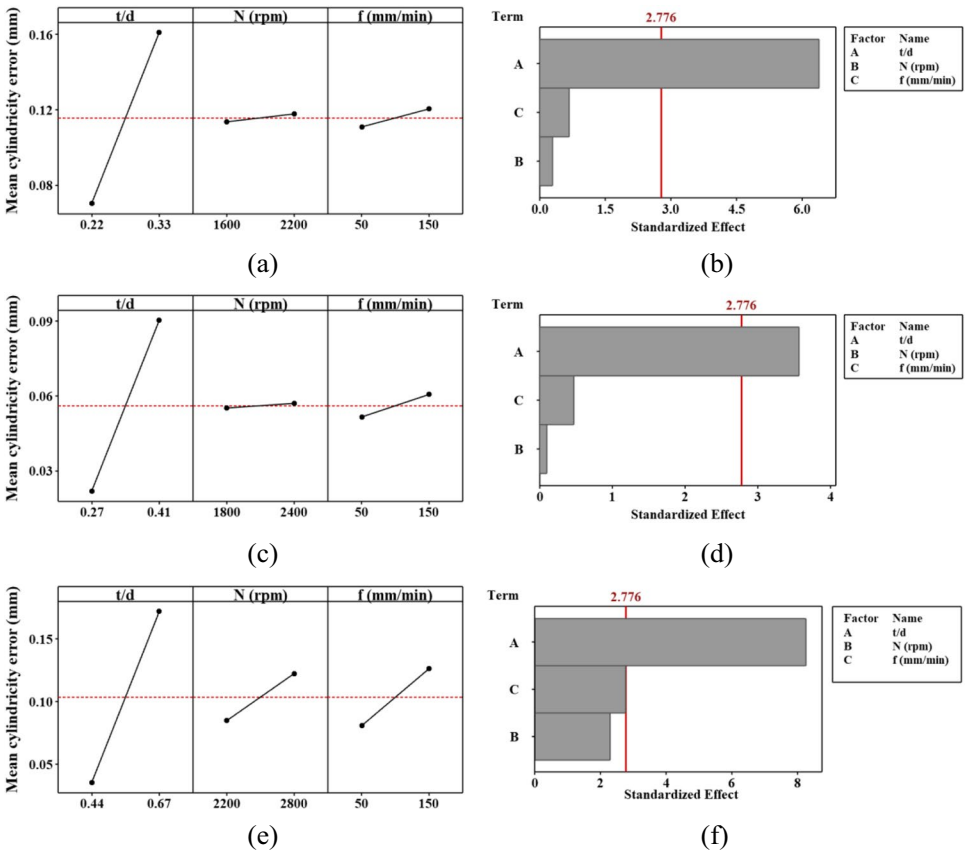

Fig. 10 Main effects plots and Pareto chart of the effets plots for mean cylindricity error. a Main effect plot for holes Ø9.2. b Pareto chart of standardized effect for holes Ø9.2. c Main effect plot for holes Ø7.3. d Pareto chart of standardized effect for holes Ø7.3. e Main effect plot for holes Ø4.5. f Pareto chart of standardized effect for holes Ø4.5

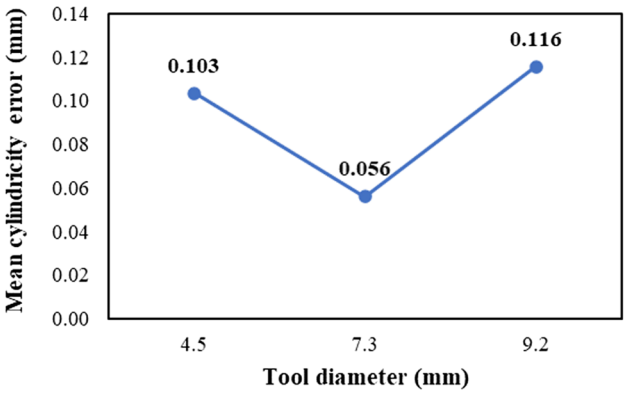

Fig. 11 Effect of different friction drills on the mean cylindricity error

Table 12 ANOVA for collar height for holes Ø4.5

Source	DF	Adj SS	Adj MS	*F*-value	*P*-value
Model	3	0.010150	0.003383	67.67	0.001
Linear	3	0.010150	0.003383	67.67	0.001
t/d	1	0.008450	0.008450	169.00	0.000
N (rpm)	1	0.001250	0.001250	25.00	0.007
f (mm/min)	1	0.000450	0.000450	9.00	0.040
Error	4	0.000200	0.000050		
Total	7	0.010350			

Model summary: $S = 0.0070711$, R-sq = 98.07%, R-sq(adj) = 96.62%, R-sq(pred) = 92.27%.

Table 13 ANOVA for collar height for holes Ø7.3

Source	DF	Adj SS	Adj MS	*F*-value	*P*-value
Model	3	0.042437	0.014146	125.74	0.000
Linear	3	0.042437	0.014146	125.74	0.000
t/d	1	0.035112	0.035112	312.11	0.000
N (rpm)	1	0.002812	0.002812	25.00	0.007
f (mm/min)	1	0.004512	0.004512	40.11	0.003
Error	4	0.000450	0.000113		
Total	7	0.042887			

Model summary: $S = 0.0106066$, R-sq = 98.95%, R-sq(adj) = 98.16%, R-sq(pred) = 95.80%

When the rotational speed increases, the temperature at the tool-workpiece interface increases [10]. As a result, the workpiece yield stress drops, the material undergoes less strain hardening, and correspondingly the collar height of the material extruded-up increases.

When the *t/d* ratio increases, the contact area between the tool and the workpiece becomes larger. Consequently, the heat generated due to friction between the tool and the workpiece rises, which causes material softening accordingly, leading to increased collar height. Finally, when the feed rate increases, the axial force increases [3]. According to Eq. (1), by increasing the axial force, the friction force increases; as a result, the collar height rises.

Table 14 ANOVA for collar height for holes Ø9.2

Source	DF	Adj SS	Adj MS	*F*-value	*P*-value
Model	3	0.86204	0.287346	69.45	0.001
Linear	3	0.86204	0.287346	69.45	0.001
t/d	1	0.72601	0.726013	175.47	0.000
N (rpm)	1	0.03251	0.032513	7.86	0.049
f (mm/min)	1	0.10351	0.103513	25.02	0.007
Error	4	0.01655	0.004137		
Total	7	0.87859			

Model summary: $S = 0.0643234$, R-sq = 98.12%, R-sq(adj) = 96.70%, R-sq(pred) = 92.47%

$$F_f = \frac{Fa}{sin\frac{\alpha}{2}} \times \mu \tag{1}$$

where F_f is the friction force, Fa is the axial force, α is the friction angle of the friction drill, and μ is the coefficient of friction.

4.4 Macro- and microstructure observations

The form tapped specimens were cut by wire EDM and prepared for the examination of the macro- and microstructures. A series of silicon carbide (SiC) papers are used to grind the specimen cross-section starting from coarse grits to fine grits (P220, P500, P1000, P1200, and P2000), and water cooled. Then, the ground specimens were polished by diamond paste and immersed in a chemical etchant consisting of 10 mL HNO_3 + 20 mL HCl + 30 mL distilled water according to ASTM E407-99 standard [17]. The chemical etchant revealed the grain boundary and showed the large plastic deformation of the work material.

The elevated temperature during both friction drilling and form tapping processes and the associated plastic deformation affect the material macro- and microstructure and refine it. The effect can appear in the different structural zones shown in Fig. 14. The Stir zone is the zone in direct contact with the tool and is affected by the elevated temperature as well as high plastic deformation. In the thermo-mechanical affected zone (TMAZ), there is no contact with the tool, but it is affected by the plastic deformation and the elevated temperature. Finally, the heat-affected zone (HAZ) is the zone affected only by the conducted heat.

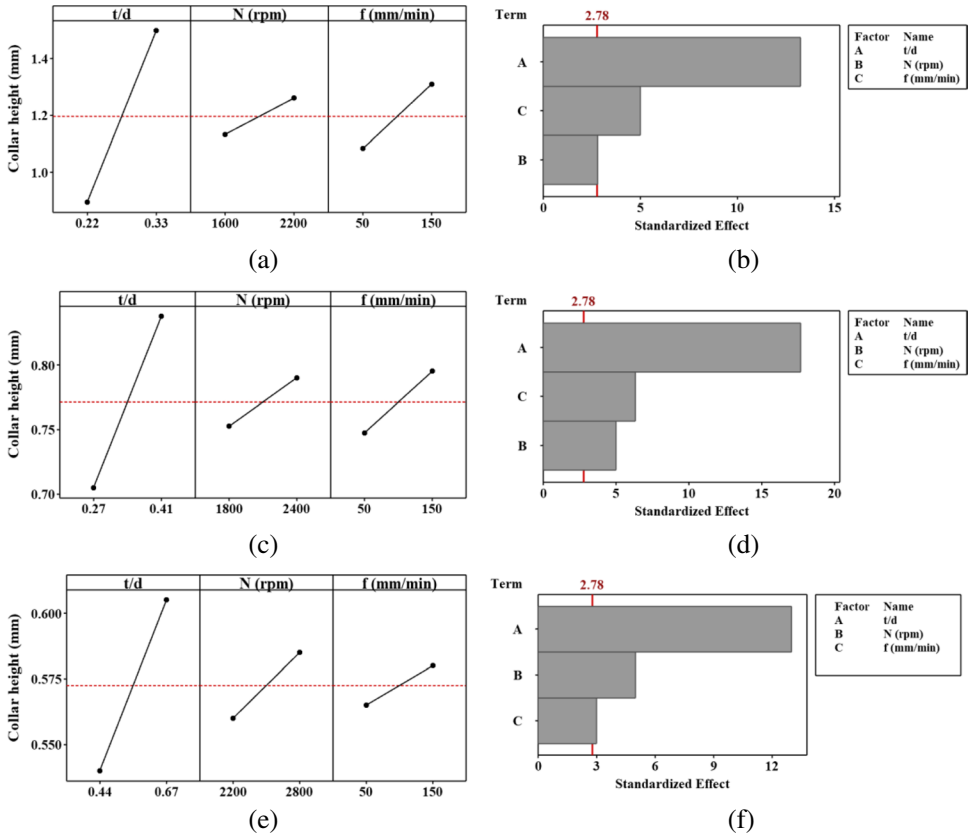

Fig. 12 Main effects plots and Pareto chart of the effets plots for collar height. a Main effect plot for holes Ø9.2. b Pareto chart of standardized effect for holes Ø9.2. c Main effect plot for holes Ø7.3. d Pareto chart of standardized effect for holes Ø7.3. e Main effect plot for holes Ø4.5. f Pareto chart of standardized effect for holes Ø4.5

Figure 15 illustrates a macrostructure of the formed thread M10X1.5 showing the location of the different micrographs observed and the crest split as a characteristic of the formed thread, which depends on the hole diameter before tapping. The crest split becomes smaller when the hole diameter is smaller [18].

Additionally, form tapping being a warm forming process leads to higher mechanical properties of the produced threaded joint through the controlled crystalline structure of the material. Form tapping is performed while the material (stainless steel 304) is below the recrystallization temperature (usually in the range of 0.3 T_m, where T_m is the melting point of the material). This reduces the force and power requirements of the form tapping and allows more intricate geometrical configurations (threads) to be produced with no need for annealing. Warm forming provides a compromise between cold forming and hot forming [19].

Form tapping as a warm forming process provides the following merits:

1. Form tapping is associated with strain hardening leading to increased hardness and strength.
2. Elongated and bent crystal flow lines, Fig. 14, that give the opportunity for desirable directional properties.

Accordingly, the produced joints exhibit higher strength and higher load carrying capacity compared to the conventionally cut joints, as will be demonstrated thereafter in this chapter.

Due to high deformation in the stir zone and elevated temperature, high grain refinement can be observed in Fig. 16, which shows that the austenite grains became coarser as moving in the direction of the base metal. In TMAZ, material layers in TMAZ displace relative to each

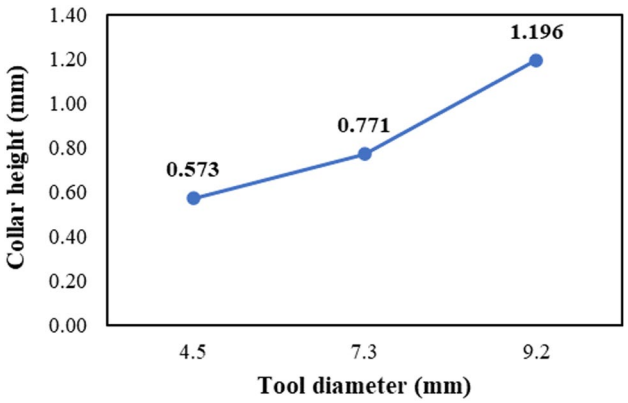

Fig. 13 Effect of different friction drills on the collar height

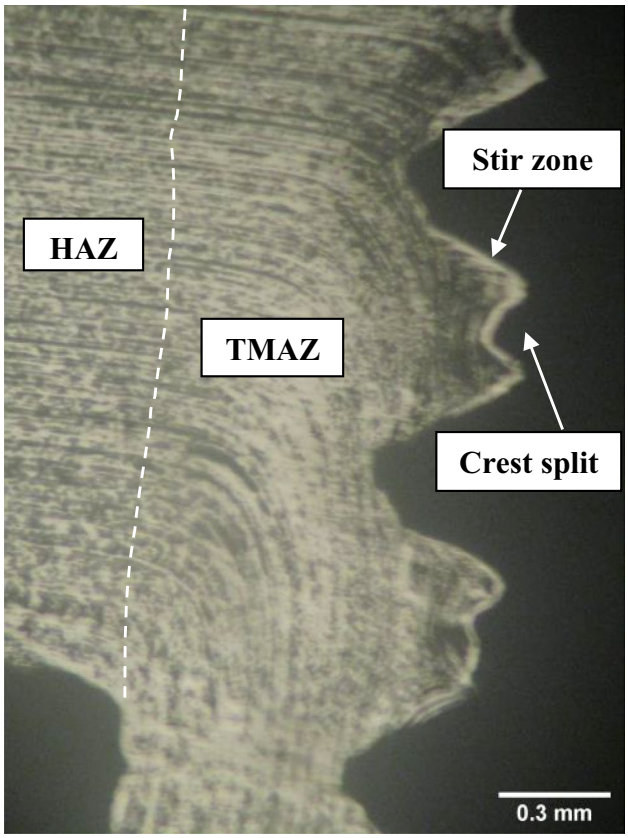

Fig. 14 Macrostructure of different structural zones for M5×0.8 formed thread (X50)

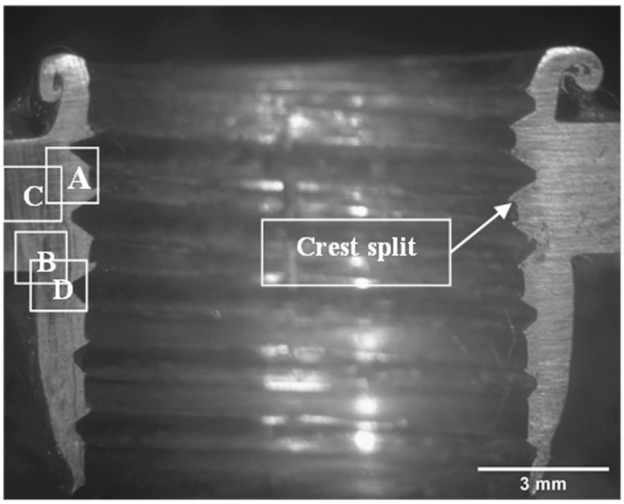

Fig. 15 Cross-section view of formed thread M10×1.5 for specimen B (X7)

other and are partially recrystallized, grains elongated, flattened, and turned upwards and downwards in the deformation direction to form a thread, as shown in Fig. 17(b, d).

Figure 17(a) shows the flowable and displacement of work material at the thread crest. The microstructure of AISI 304 stainless steel is characterized by austenite grains surrounded by δ-ferrite stringers, carbides at grain boundaries, and precipitated carbides particles [20, 21]. Notably, many carbide particles were found at the TMAZ and reduced by moving away toward the base metal due to elevated temperature at this zone, Fig. 17(d).

4.5 Micro-hardness measurements

It should be accounted that the work material has been subjected consecutively to two processes, which are friction drilling, and form tapping. The friction drilling was performed dry (without cooling) as previously mentioned; the material was subjected to a severe plastic deformation leading to an increase in its temperature to about half and two-thirds of its melting point. A form tapping process followed the friction drilling. Both processes have considerably affected the hardness as well as the macro- and microstructure of work material (specimen).

To measure the hardness after form tapping, the specimens were cut longitudinally by wire EDM. Their cross-sections were ground to eliminate the effect of surface roughness and then polished to facilitate the hardness test. Using the Vickers hardness tester, nine points were taken at different positions, as illustrated in Fig. 18, to examine the three regions, TMAZ, HAZ, and BM. A right pyramid diamond indenter with a square base and an angle of 136° between its opposite faces was used, applying a load of 0.3 Kgf for 10 s, and the indention depth was measured.

The hardness plots of the form tapped threads M8×1.25 and M5×0.8 for both AISI 304 specimens A and B at the shown working conditions have the same trend starting from TMAZ (located at 0.5 mm from the teeth crest). All plots attain a maximum value at HAZ (located at 2 mm from teeth crest), then reduced by getting away from teeth crest at the base material locations 4, 5.5, and 7 mm, respectively, Figs. 19 and 20. As a result of the carbide precipitation and the grain refinement occurred during the deformation, as mentioned in the microstructure observations.

Such behavior can be attributed that at the TMAZ location, the material of the specimen attains the highest temperature due to the plastic deformation taking place during the friction drilling process. Consequently, the material becomes strain hardened and gets harder than the base material, Figs. 19 and 20. Accordingly, the material approaches the recrystallization temperature and attains a coarse-grained microstructure of a hardness greater than that of the base material due to the strain hardening effect. However, during the form tapping process, the material becomes soft due to the subsequent heating effect involved in the form tapping process; therefore, the hardness at TMAZ is lower than at the HAZ.

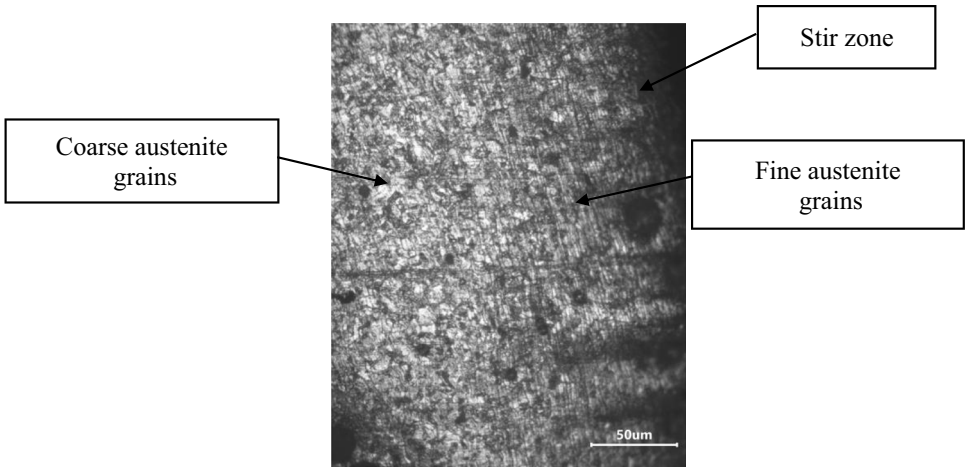

Fig. 16 Optical micrograph of formed thread M10 × 1.5 (X100)

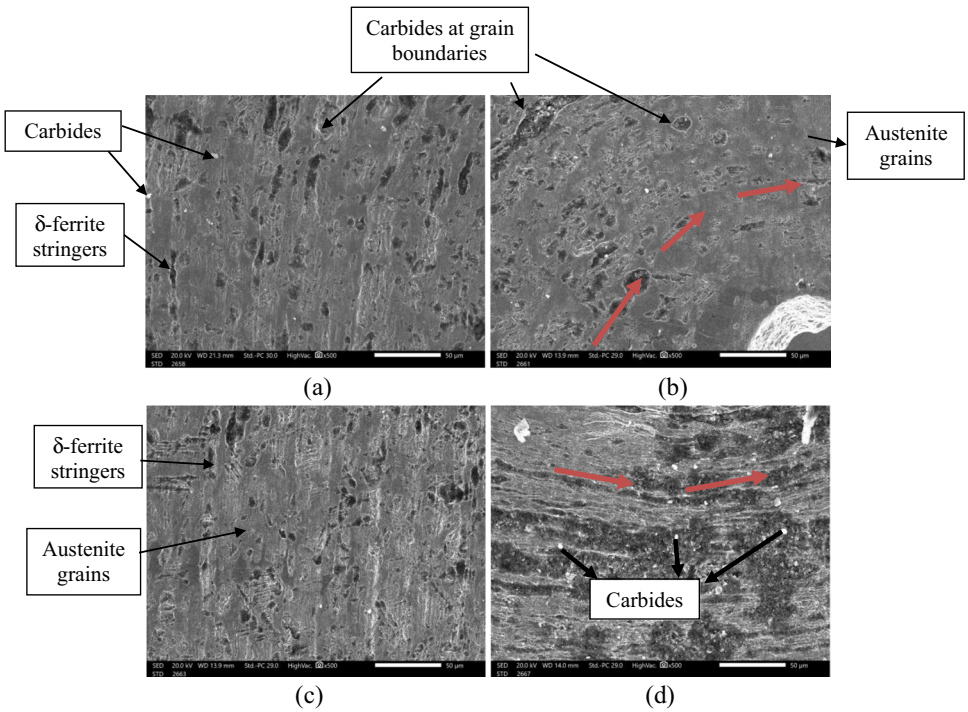

Fig. 17 Optical micrographs of formed thread M10 × 1.5 (X500) (**a**) at cross-section location A, (**b**) at cross-section location B, (**c**) at cross-section location C, (**d**) at cross-section location D

In the HAZ location, the temperature is less than the recrystallization temperature giving a strain-tempered fine-grained microstructure, consequently attaining maximum hardness after cooling. Finally, the hardness approaches more or less that of the base material, which has not affected or strained mechanically or thermally, Figs. 19 and 20.

It is also important to remark that the hardness plots of specimens B ($t = 3$ mm) overside those of specimens A ($t = 2$ mm) for both threads M8 × 1.25 and M5 × 0.8, Figs. 19 and 20. This can be attributed to the greater cooling rate, realized in the case of specimens B of greater thickness ($t = 3$ mm), acting as a greater heat sink. Hence, specimen B realizes higher cooling rates than those realized by specimens A ($t = 2$ mm) and, consequently, higher hardness plots, Figs. 19 and 20.

Comparing the conventional cut and formed tapped holes in Figs. 19 and 20, it is noticeable that the hardness values for the conventional form tapped at the different zones are approximately the same. As a result of the usage of cooling in twist drilling and cut tapping processes, therefore the process temperature is reduced, and the effect of heat on hardness is neglected.

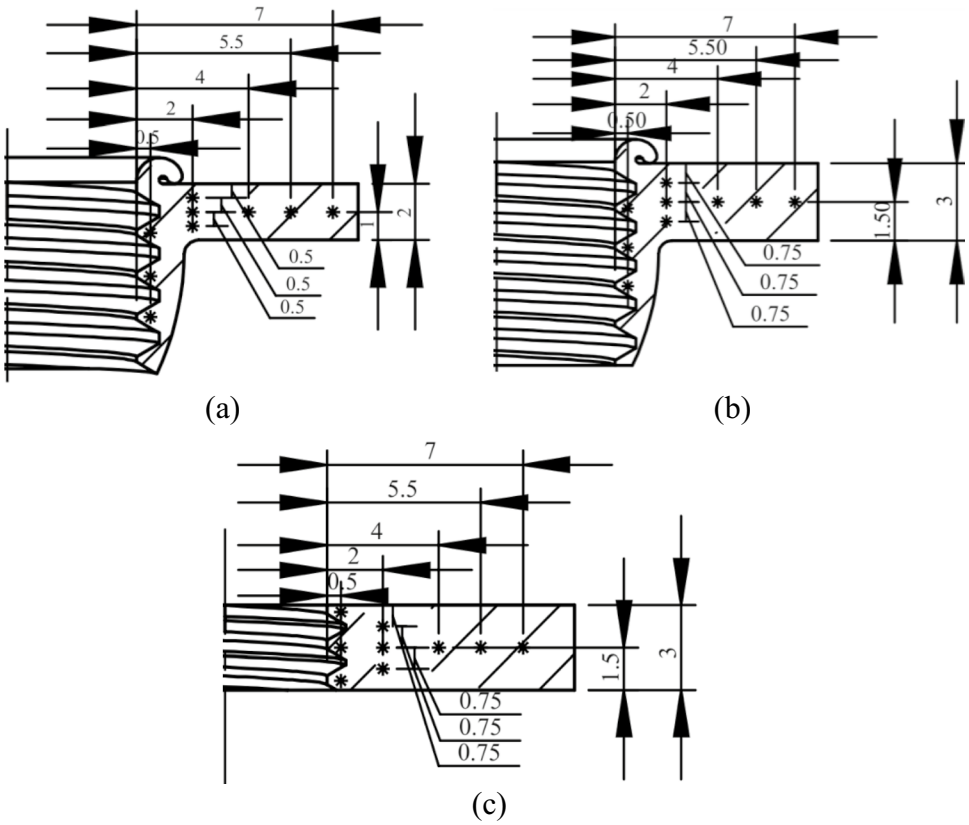

Fig. 18 Micro-hardness test points for a formed thread specimen A, b formed thread specimen B, c cut thread specimen B

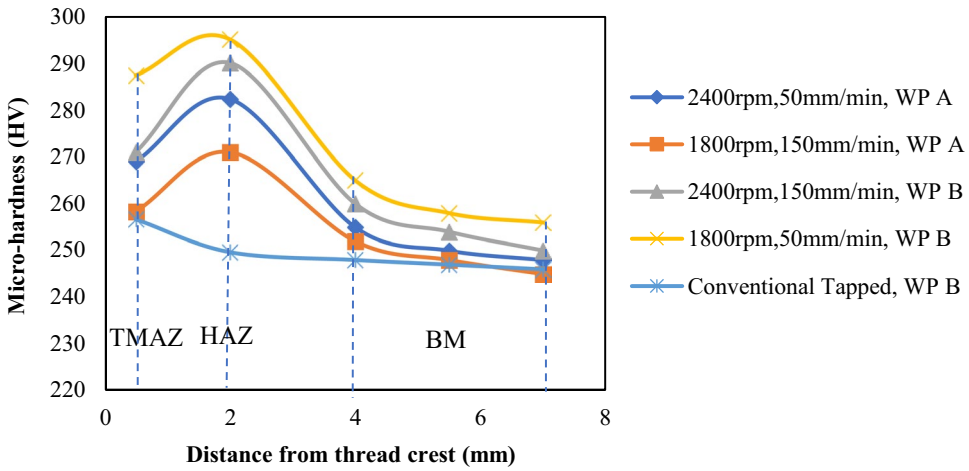

Fig. 19 Microhardness plots for formed thread M8 × 1.25

4.6 Comparison between formed tapped joints and conventional tapped joints regarding ultimate tensile loads

After the friction drilling process, the form tapping process was conducted, and the joint strength was compared with the conventional joint strength. First, it is noticeable that the effective thread length obtained from conventional drilling with a twist drill and cutting tap was about 1–3 threads. Then, by comparing the performance of the two methods, the results show that the formed tapped joint realizes a higher ultimate tensile load as compared to the cut tapped joint for both specimens A and B. Figure 21 clarifies that the ultimate load of the cut tapped joint for specimen A is lower than the formed tapped joint by 78.49%, 74.6%, and 50.96% for thread M10 × 1.5, M8 × 1.25, and M5 × 0.8 respectively. However, specimen B is lower by 45%, 62.76%, and 60% for thread M10 × 1.5, M8 × 1.25, and M5 × 0.8, respectively. The reason is that the effective length of the formed thread is longer than the cut thread, which increases joint strength.

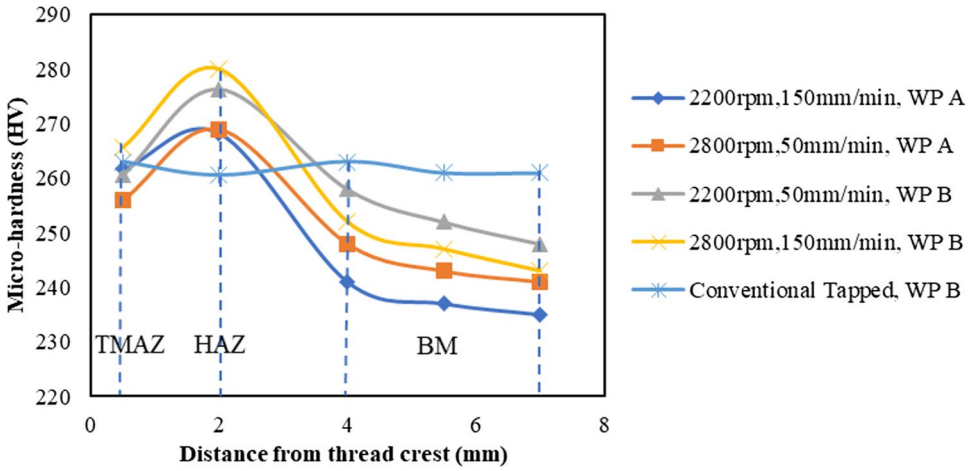

Fig. 20 Microhardness plots for formed thread M5 × 0.8

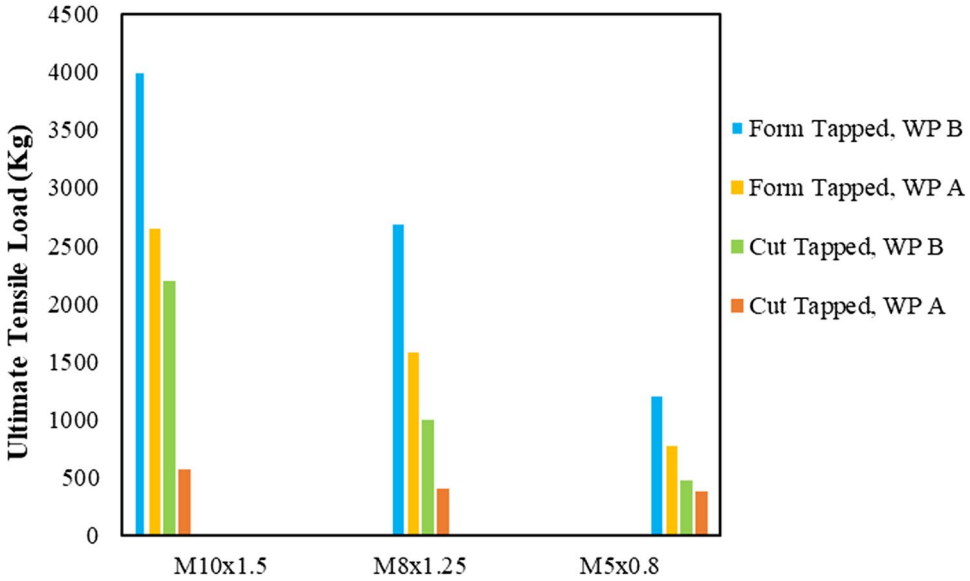

Fig. 21 Bar chart of the ultimate tensile load for form and cut tapped holes of specimens A and B

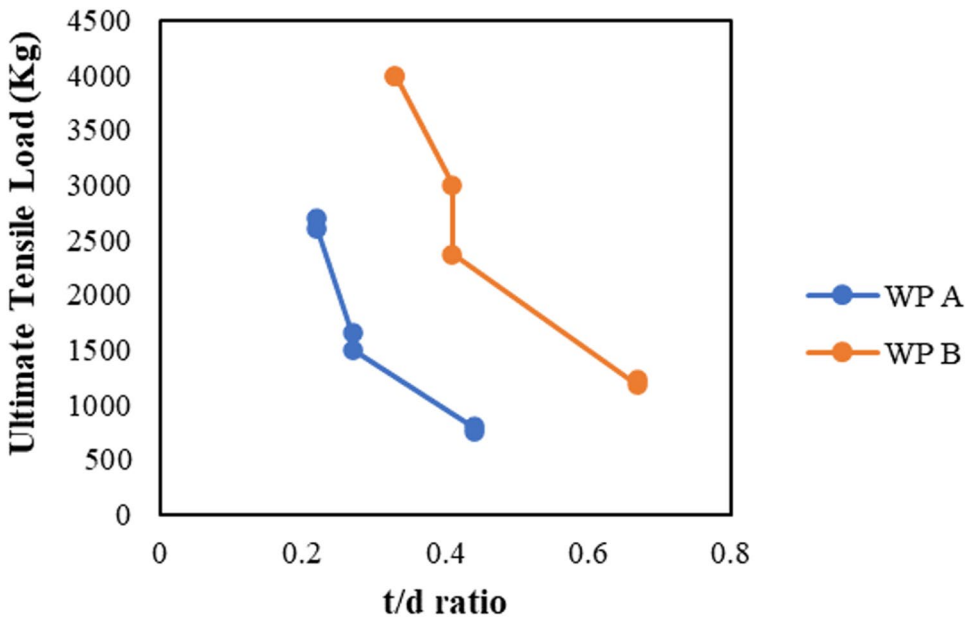

Fig. 22 Effect of t/d ratio on the ultimate tensile load of the form tapped thread

Increasing the *t*/*d* ratio leads to a decrease in the joint strength for the different specimen's thicknesses, as shown in Fig. 22. It means that the thread diameter decreases; therefore, the contact area decreases, and the required force for joint failure decreases.

The formed thread failed by applying the tensile load due to thread shearing. However, the breakage of the formed thread M8 × 1.25 of specimen B ($N = 2400$ rpm, and $f = 150$ mm/min) happens at the stud and realizes the best performance.

5 Conclusion

This research paper conducted experimental investigations on friction drilling followed by form tapping of austenitic stainless steel AISI 304. In friction drilling, a set of experiments were performed to explore the effects of *t*/*d* ratio, spindle speed (*N*), and feed speed (*f*) on mean hole diametral oversize (*U*), mean cylindricity error, and collar height. Then, the form tapping process was performed to examine the thread quality in terms of hardness and metallographic structure and compare the conventional joint produced by twist drill, cutting tap, and the other joint produced by friction drill and form tap. The most salient results of this research are listed as follows:

- Increasing the *t*/*d* ratio means that a large amount of the work material was formed, inducing more frictional heat conducted to the workpiece, which softened and deformed the metal, decreasing the mean hole diametral oversize and increasing the collar height.
- The mean hole diametral oversize decreased by increasing the input working parameters (*t*/*d* ratio, *N*, and *f*).
- It is noticeable that the friction drill Ø7.3 provided by Formdrill Company (Belgium) realized the minimum mean hole diametral oversize and cylindricity error compared to the locally made tools Ø9.2 and Ø4.5, since it has the lowest overhang ratio compared to the other tools.
- The collar height was significantly affected by the input working parameters (*t*/*d* ratio, *N*, and *f*) using the different friction drill diameters. Increasing those parameters leads to an increase in the collar height. However, the *t*/*d* ratio had the most significant influence on the collar height.
- Concerning the hole cylindricity error point of view, the *t*/*d* ratio was the only significant factor that affected the mean cylindricity error. When the *t*/*d* ratio increased, the axial force increased, which enhanced the cylindricity error.
- Finer austenite grains surrounded by δ-ferrite stringers were observed near to thread crest and became coarser by moving toward the base metal.
- Many carbide particles precipitated at the TMAZ due to the elevated temperature during the deformations process.
- The higher hardness values were presented at the HAZ, which had strain-tempered fine-grained microstructure and carbides due to the temperature at this location being less than the recrystallization temperature. However, the hardness at the TMAZ is less than that at the HAZ due to softening work material during the form tapping process.
- The hardness of conventional tapped threads at different zones was approximately the same and no material softening occurred due to the usage of a cooling medium.
- Specimen B ($t = 3$ mm) acts as a greater heat sink; therefore, its hardness plots override those of specimen A ($t = 2$ mm).
- The joint strength of the formed thread was higher than the conventionally machined or cut thread due to the longer effective thread length obtained from the friction drilling process.

Acknowledgements The authors would like to acknowledge Formdrill Company in Belgium for offering the Ø7.3 friction drill and its form tap (M8x1.25). Thanks is due to Dr. Mohamed Abd-Alrazzaq for his contribution to analyzing the microstructures of the formed thread.

Author contribution Professor Helmi Youssef contributed to the critical revision and editing of the manuscript. Professor Mohammad Al-Makky initiated the research point and participated in the manuscript's revision and editing. Professors Youssef and Al-Makky also contributed to analyses of macro- and microstructure and the associated changes in micro-hardness. Eng. Nada Abdelmoneim conducted the experiments, analyzed the results, extracted the conclusions, and wrote the manuscript. All authors approved the manuscript to be published.

Funding Open access funding provided by The Science, Technology & Innovation Funding Authority (STDF) in cooperation with The Egyptian Knowledge Bank (EKB). Open access funding is provided by The Science, Technology & Innovation Funding Authority (STDF) in cooperation with The Egyptian Knowledge Bank (EKB). The authors declare that this study did not receive any funding to reach this conclusion.

Data availability The manuscript includes all data.

Declarations

Conflict of interest The authors declare no competing interests.

References

1. Demir Z, Özek C, Bal M (2018) An experimental investigation on bushing geometrical properties and density in thermal frictional drilling. Appl Sci 8(12):2658. https://doi.org/10.3390/app8122658
2. Miller SF, Shih AJ (2006) Friction drilling: a chipless hole-making process. In international manufacturing science and engineering conference, vol 47624, pp 911–918
3. El-Bahloul SA, El-Shourbag HE, & El-Midany TT (2016) Effect of tool geometry, feed rate, and rotational speed of thermal friction drilling process on AISI 304 stainless steel. Mansoura Engineering Journal 41(1):9–15
4. Chow H-M, Lee S-M, Yang L-D (2008) Machining characteristic study of friction drilling on AISI 304 stainless steel. J Mater Process Technol 207(1–3):180–186. https://doi.org/10.1016/j.jmatprotec.2007.12.064
5. Ku W-L, Hung C-L, Lee S-M, Chow H-M (2011) Optimization in thermal friction drilling for SUS 304 stainless steel. Int J Adv Manuf Technol 53(9–12):935–944
6. El-Bahloul SA, El-Shourbagy HE, El-Bahloul AM, El-Midany TT (2018) Experimental and thermo-mechanical modeling optimization of thermal friction drilling for AISI 304 stainless steel. CIRP J Manuf Sci Technol 20:84–92. https://doi.org/10.1016/j.cirpj.2017.10.001
7. Dehghan S, Soury E, Ismail MISb (2021) A comparative study on machining and tool performance in friction drilling of difficult-to-machine materials AISI304, Ti-6Al-4V, Inconel718. J Manuf Process 61:128–152. https://doi.org/10.1016/j.jmapro.2020.10.078
8. Sobotová L, Kmec J, Bicejová L (2011) Thermal drilling-new progressive technology. Annals of the Faculty of Engineering Hunedoara 9(3):371
9. Somasundaram G, Rajendra Boopathy S, Palanikumar K (2011) Modeling and analysis of roundness error in friction drilling of aluminum silicon carbide metal matrix composite. J Compos Mater 46(2):169–181. https://doi.org/10.1177/0021998311410493
10. Ozler L, Dogru N (2013) An experimental investigation of hole geometry in friction drilling. Mater Manuf Processes 28(4):470–475. https://doi.org/10.1080/10426914.2012.746699
11. Özek C, Bal M (2020) Investigation of parameters affecting the formation of the bushing and bushing wall obtained in the friction drilling process. Pamukkale Univ J Eng Sci 26(4):620–627
12. Urbikain G, Perez JM, López de Lacalle LN, Andueza A (2018) Combination of friction drilling and form tapping processes on dissimilar materials for making nutless joints. Proc Inst Mech Eng, Part B: J Eng Manuf 232(6):1007–1020. https://doi.org/10.1177/0954405416661002
13. Sarafraz Y, Koch A, Felinks N, Biermann D, Walther F (2021) Influence of pre-drilling on hardness and tensile failure of formed internal threads in thin-walled AZ91 cast alloys. Eng Fail Anal 130:105783. https://doi.org/10.1016/j.engfailanal.2021.105783
14. Wu H, Clarke R, Porter M, Ward R, Quinn J, McGarrigle C, McFadden S (2021) Thread-stripping test procedures leading to factors of safety data for friction-drilled holes in thin-section aluminium alloy. Thin-Walled Structures 163:107653. https://doi.org/10.1016/j.tws.2021.107653
15. Miller SF, Tao J, Shih AJ (2006) Friction drilling of cast metals. Int J Mach Tools Manuf 46(12–13):1526–1535. https://doi.org/10.1016/j.ijmachtools.2005.09.003
16. Pantawane PD, Ahuja BB (2014) Parametric analysis and modelling of friction drilling process on AISI 1015. Int J Mechatron Manuf Syst 7(1):60–79
17. Standard A. E407–99 Standard practice for microetching metals and alloys. West Conshohocken, PA: American Society for Testing and Materials ASTM International.
18. Fromentin G, Poulachon G, Moisan A, Julien B, Giessler J (2005) Precision and surface integrity of threads obtained by form tapping. CIRP Ann 54(1):519–522. https://doi.org/10.1016/s0007-8506(07)60159-0
19. Youssef HA, El-Hofy HA, & Ahmed MH (2012) *Manufacturing technology: materials, processes, and equipment*: CRC-Press. https://books.google.com.eg/books?hl=en&lr=&id=gcpOPFO_Qg8C&oi=fnd&pg=PP1&ots=T2YvutRcAQ&sig=n0xlk9dxmIWHFUO92TB007bDBk&redir_esc=y#v=onepage&q&f=false
20. Llewellyn D, & Hudd R (1998) *Steels: metallurgy and applications*: Elsevier. https://books.google.com.eg/books?hl=en&lr=&id=Wl1azjcJbIIC&oi=fnd&pg=PP1&dq=Steels:+metallurgy+and+applications&ots=_eLQkVxmc0&sig=gpbnmXqzrUUb-Ohk5OFx8TyQUow&redir_esc=y#v=onepage&q=Steels%3A%20metallurgy%20and%20applications&f=false
21. Vander Voort GF, Lampman SR, Sanders BR, Anton GJ, Polakowski C, Kinson J., . . . Scott Jr WW (2004). *ASM handbook* (Vol. 9).